EPJ Web of Conferences **308**, 06004 (2024) https://doi.org/10.1051/epjconf/202430806004
ISRD 17

Fast and thermal neutron spectrum dosimetry measurements in the Advanced Test Reactor large-B and small-I positions following the sixth core internals change-out

Michael Reichenberger[1,*], *Andrew* Maile[2], *Matthew* Johnson[2], *Daren* Norman[2], *Samuel* Bays[3], *Kelly* McCary[1], and *Nathan* Manwaring[2]

[1]Idaho National Laboratory, Energy and Environment Science and Technology, 1955 N Fremont Ave, Idaho Falls, ID 83415, USA
[2]Idaho National Laboratory, Advanced Test Reactor, 1955 N Fremont Ave, Idaho Falls, ID 83415, USA
[3]Idaho National Laboratory, Nuclear Science and Technology, 1955 N Fremont Ave, Idaho Falls, ID 83415, USA

Abstract. The Advanced Test Reactor (ATR) has a wide variety of irradiation positions that have had experiments that were developed by users from around the world. Most experiment irradiations rely on thoroughly benchmarked numerical models. However, some irradiation positions in ATR are not as well- characterized and are complicated by spectral perturbations from control cylinder orientation. The "small I" and "large-B" irradiation positions are located nearby control cylinders and suffer from these flux perturbations from control cylinder orientations that change during an irradiation cycle to maintain the desired core power distribution. Models predicted that these types of position would exhibit both spectral shifts and amplitude changes in neutron flux, but few measurements have been conducted to benchmark these predictions. Recently, requalification testing was performed to confirm the operational readiness of the ATR following the completion of the Core Internals Change-out (CIC). These tests provided a unique opportunity to validate the analytical methods used to simulate the ATR because nearly all components in the reactor were in a clean as-built state, significantly reducing modelling uncertainties. One subset of the testing included characterization of the fast and thermal neutron flux in the "small-I" and "large-B" positions using silver, cobalt, and nickel neutron dosimetry. In contrast to typical irradiation cycles, the control cylinders were held in position during the post-CIC nuclear testing. The specific activity of these dosimeter wires was measured following two low-power tests with different control cylinder positions.

* Corresponding author: michael.reichenberger@inl.gov

1 Introduction

The Advanced Test Reactor (ATR) is a versatile nuclear research reactor located at the Idaho National Laboratory (INL) in eastern Idaho, United States. It is one of the most powerful and flexible research reactors in the world and is primarily used for materials testing, isotope production, and basic nuclear science research. The ATR is a light-water-cooled, beryllium-moderated reactor with a nominal thermal power capacity of 250 MW utilizing specially designed fuel, arranged in a serpentine pattern to create 9 flux traps, illustrated in Fig. 1. The special design of ATR allows for the neutron flux in flux traps to be controlled locally by 16 outer shim control cylinders (OSCCs), providing flexibility for experiment programs and allowing experiments with different dose requirements to be irradiated concurrently. There are numerous additional irradiation locations within the ATR. The "B-positions" are situated between the OSCCs and the driver fuel while the "I-positions" are located outside the OSCCs, illustrated in Fig. 1. Unlike the flux traps, most experiments located in the B- and I-positions are "drop-in" experiments with limited instrumentation (if any). For this reason, it is critical to have a fundamental understanding of the typical neutron flux and the impact of OSCC position in these irradiation locations. The expected neutron flux in most experiments in ATR is determined by simulation and modelling of the anticipated reactor conditions. These methods are validated using measured results from numerous previous cycles. However, validation with unirradiated core components is rarely possible.

The ATR undergoes regular maintenance and refurbishment activities to ensure safe and reliable operation. One of the major maintenance activities performed on the ATR is the core internals change-out (CiC), which involves replacing the various components that make up the reactor core. The ATR CiC consists of numerous different components, including the structural elements that hold the fuel and control mechanisms, the OSCCs and shim-control rods with their associated controls systems, and significantly, the beryllium reflector. These components must be periodically replaced as they deteriorate under the intense radiation dose they receive to ensure that the reactor operates safely and efficiently. The most recent CiC-VI activities were in completed 2022. The presence of all-new hardware (most importantly the reflector) in the reactor necessitates extensive nuclear testing (NTs) to ensure that ATR safety basis requirements are met prior to full-power operations [1]. These NTs included several low-power, relatively short irradiations that were used to activate various types of dosimeters to assess critical reactor parameters (such as element and lobe power distributions). Most notably, the lobe power monitoring system was calibrated during nuclear testing. Although not an integral part of the NTs, additional dosimetry was deployed into B- and I- positions to verify prior calculations of neutron flux levels and to assess the impact of OSCC position in these heavily utilized irradiation locations.

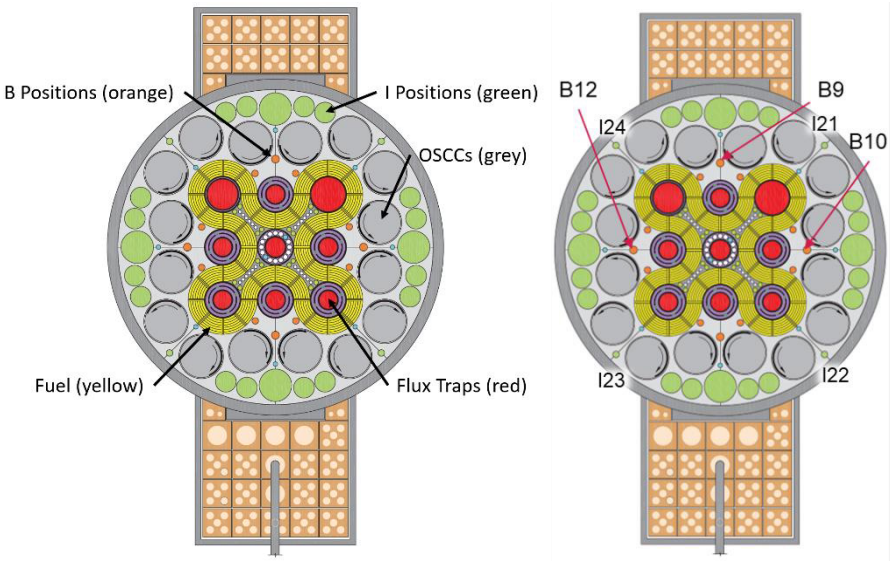

Fig. 1. The ATR core is composed of fuel elements arranged in a serpentine pattern to create 9 flux traps (left) the specific irradiation positions of interest are identified (right) [2].

2 Method

Flux Monitor Wire Holders (FMWHs) were assembled such that the dosimeter wires were situated at the core centreline plane of the ATR *after* installation. This required several variations on the basic design illustrated in Fig. 2. An aluminium spacing wire was used to position an aluminium capsule at the core centreline. The length of the spacer wire was varied to ensure proper spacing after installation for each FWMH. Within the aluminium capsule resided a 0.1% cobalt in aluminium wire, a pure silver wire, and a nominal 97% nickel wire described in Table I. These dosimeters were selected to correspond with ASTM standards E481 and E264 respectively [3], [4]. The neutron absorption cross-sections for the reactions of interest are shown in Fig. 3. From these cross-sections it is clear that the cobalt is predominantly sensitive to thermal neutrons, however a large resonance for epithermal neutrons exists. For that reason, silver is also irradiated which also has a large epithermal neutron cross-section at a lower energy than for cobalt and a relatively smaller cross-section for thermal neutron absorption. Nickel has a threshold around 1 MeV for neutron absorption and is therefore used for measurement of > 1-MeV neutrons.

Table I. Description of dosimeter wires.

Wire Material	*Purity*	*Length*	*Diameter*	*Purpose*
Cobalt / Aluminium	0.1% Co 99.9% Al	½”	0.0316”	Thermal Neutrons
Silver	99.99%	¼”	0.020”	Epithermal Neutrons
Nickel	97%	¼”	0.020”	> 1 MeV Neutrons

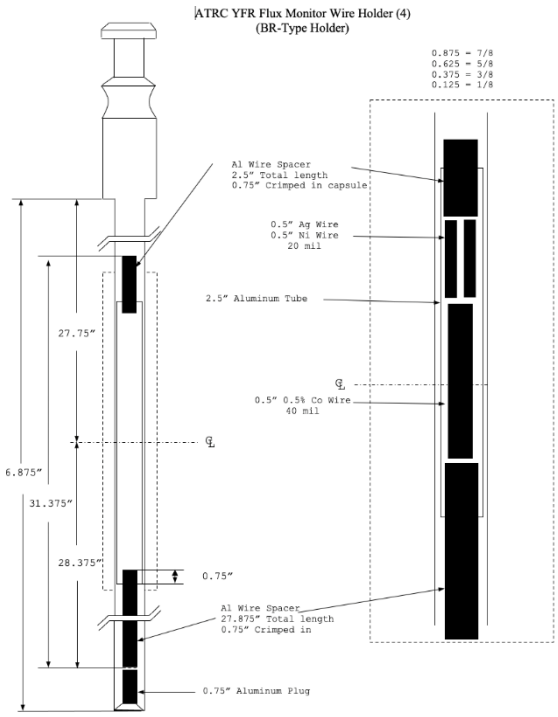

Fig. 2. Example FMWH diagram depicting the assembly of holders to position the dosimetry wires at the core centreline.

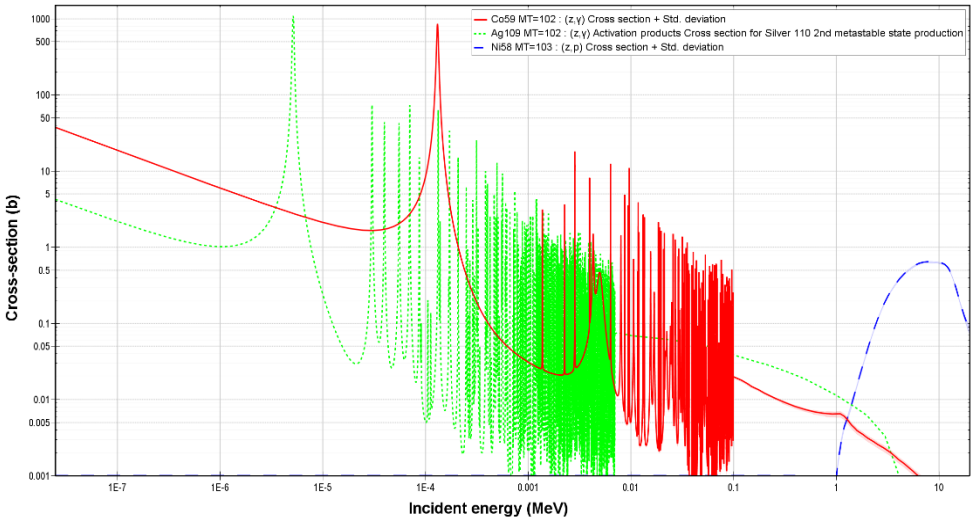

Fig. 3. Neutron absorption cross-sections for the reactions of interest [5][6].

Two irradiations were performed for this experiment: CiC-6 and CiC-7, summarized in Table II and illustrated in Fig. 4. Under normal operations total core power is monitored by multiple systems. Due to the experimental nature of the nuclear testing following CiC, these systems were not calibrated but the corrected lobe powers were determined following the completion of nuclear testing. The major distinction between CiC-6 and CiC-7 was the final OSCC positions which were adjusted during CiC-6 to shift power dramatically into the south half of the reactor but that were left balanced during CiC-7. The OSCC positions and

corrected lobe and total core power are illustrated in Fig. 4 and summarized in Table III. Both cycles lasted for a nominal 2-hour period at the desired power with minimal adjustment of the OSCCs. The relatively low-power and short irradiation period yielded sufficiently low fluence to neglect burnup of activation products in the dosimeters and produced samples with activities low enough to handle with only minimal contamination and radiation protection constraints.

Table II. NT-6 Cycle Details [1].

Cycle	*Criticality*	*Average Critical Shim Position*	*Scram*	*Primary Coolant Inlet Temperature*	*Regulating Rod Positions*
170CiC-6	18 Oct. 2022, 16:31	64.55°	18 Oct. 2022, 19:33	92.5 °F	Full Out
170CiC-7	26 Oct. 2022, 13:12	64.53°	26 Oct. 2022, 15:38	93.0 °F	Full Out

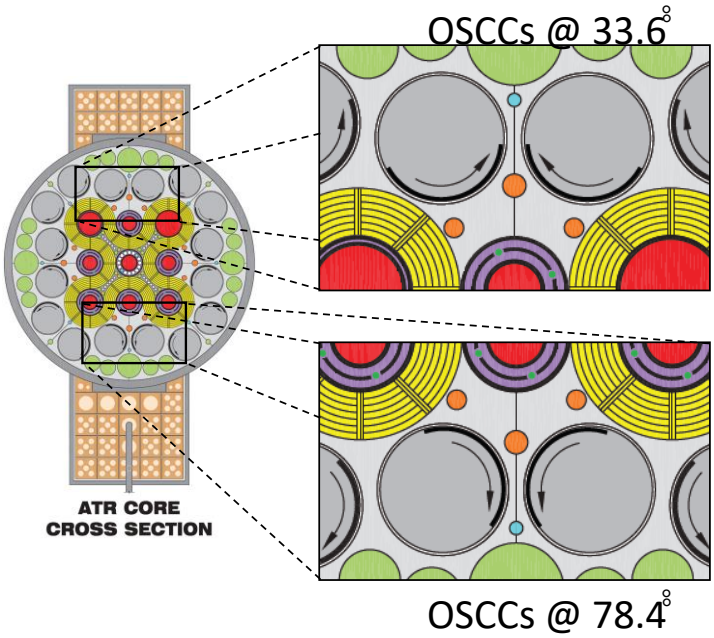

Fig. 4. The rotation of the OSCCs moves the hafnium absorber in proximity to the large-B positions.

Table III. The OSCCs were adjusted for CiC-6 to push power into the south of the reactor [1].

OSCC Pairs	*CiC-6 Position*	*CiC-7 Position*	
NW / NE	33.6°	65°	
SW / SE	78.4°	65°	
Lobe	*CiC-6 Power (MW)*	*CiC-7 Power (MW)*	*Power Ratio (7/6)*
NW	0.2650	0.2665	1.01
NE	0.2775	0.2606	0.94
C	0.4331	0.3317	0.77
SW	0.4710	0.3120	0.66
SE	0.4545	0.2931	0.64
Total	**1.9011**	**1.4639**	**0.77**

Following each irradiation, all the dosimeter wires were removed from their respective FMWH, weighed, and secured onto individual sample cards to allow for accurate positioning during measurement, depicted in Fig. 5. Each of the wires were then measured on each of 12 High-Purity Germanium (HPGe) gamma-ray spectrometers for a total of 504 measurements (12 measurements of each of 42 wires between 2 irradiations). Each HPGe detector is regularly maintained and assured to be within quality control limits by the RML quality assurance program. However, it was suspected that the various detectors could have un-identified biases associated with the efficiency calibrations and sample configurations. For this reason, the average value and standard deviation of the suite of measurements of each wire was found. Outliers were rejected based on a variance of the specific activity from the mean value for each wire greater than 3 standard deviations. Such biases were identified in two detectors (A4 and B5) using this method. Therefore, the measurement results from the remaining 10 detectors were used to determine the final measurement results. The standard deviation of the measurements across all 10 detectors was used to determine the uncertainty of the measurements and combined with the documented mass uncertainty of the balance to account for all sources of uncertainty.

Fig. 5. Dosimeter wires were fixed within a standard geometry following irradiation.

All the cobalt and nickel wires were measured 0-cm from the detector face because of the low-activity of the wires. However, the activity of the silver wires was sufficient to allow measurement at 10-cm. It was identified that the true-coincidence rate for the cobalt wires was significant because of the relatively high efficiency of the HPGe at a source distance of 0-cm. Therefore, the Co-60 activities each had a correction factor applied according to eq. 1, summarized in

Table IV, ranging from 2.5% to 6.8% (depending on detector efficiency). The results presented in Table V and Table VI include the correction for true coincidence.

$$C = \frac{1}{\prod_i^n (1 - q_i \varepsilon_i)} \qquad \textbf{Eq. (1)}$$

Where:

C	=	correlated summing correction to be applied to the measured count rate,
n	=	number of gamma or X rays in correlation with gamma ray of interest,
i	=	identification of correlated photon,
ε_i	=	total detection efficiency of i^{th} correlated photon, and
q_i	=	fraction of the gamma ray of interest in correlation with the i^{th} photon. $q_{1173\ keV} = 0.9985$ and $q_{1332\ keV} = 0.99983$ [7]

Table IV. Coincidence Correction Factors for Co-60 Measurements at RML.

Detector	*1173 keV Eff.*	*1332 keV Eff.*	*C*
A1	0.01480	0.01701	1.033
A2	0.01399	0.01213	1.027
A3	0.02442	0.0213	1.047
A4	0.01949	0.01711	1.038
B2	0.01293	0.01118	1.025
B5	0.02602	0.02289	1.057
SC	0.03352	0.03018	1.067
E2	0.02829	0.02466	1.056
E1	0.02353	0.02048	1.045
A6	0.02316	0.02019	1.045
B3	0.03446	0.03009	1.068
D4	0.03008	0.02907	1.062

3 Results

The following tables V and VI summarize the measurement results for 0.1% cobalt, pure nickel, and pure silver wires that were irradiated in the large-B and small-I positions in ATR during cycles CiC-6 and CiC-7. All specific activities are reported per unit *wire* mass to simplify comparison to the reaction rate simulation results which were presented in the same units. The reported 2σ standard deviations refer to the variation of the 10 measurements of each wire whereas the combined 2σ includes both the standard deviation of measurements and the mass uncertainty of 0.00018 g.

Table V. Results of cycle CiC-6 (NT-6-2).

Location	*Holder*	*Material*	*Mass (g)*	*Mass Unc. (%)*	*Specific Activity (uCi/g)*	*2σ Std. Dev. (uCi/g)*	*2σ Std. Dev. (%)*	*Combined 2σ (%)*
B-9	IR-67	0.5" 0.1% Co	0.02258	0.80%	3.87E-01	2.54E-02	6.56%	6.61%
B-10	IR-68	0.5" 0.1% Co	0.02225	0.81%	5.84E-01	4.08E-02	6.99%	7.04%
B-12	IR-69	0.5" 0.1% Co	0.02208	0.82%	6.06E-01	3.27E-02	5.40%	5.46%
I-21	IR-70	0.5" 0.1% Co	0.02247	0.80%	1.88E-01	1.15E-02	6.13%	6.18%
I-22	IR-71	0.5" 0.1% Co	0.02266	0.79%	5.74E-01	3.66E-02	6.37%	6.42%
I-23	IR-72	0.5" 0.1% Co	0.02233	0.81%	5.85E-01	3.15E-02	5.38%	5.44%
I-24	IR-73	0.5" 0.1% Co	0.02265	0.79%	2.06E-01	1.35E-02	6.52%	6.57%
B-9	IR-67	0.25" Ni	0.01179	1.53%	4.66E+00	2.24E-01	4.81%	5.04%
B-10	IR-68	0.25" Ni	0.01193	1.51%	6.61E+00	3.26E-01	4.92%	5.15%
B-12	IR-69	0.25" Ni	0.01192	1.51%	6.71E+00	4.30E-01	6.42%	6.59%
I-21	IR-70	0.25" Ni	0.01181	1.52%	5.23E-01	2.94E-02	5.63%	5.83%
I-22	IR-71	0.25" Ni	0.01214	1.48%	1.23E+00	7.80E-02	6.35%	6.52%
I-23	IR-72	0.25" Ni	0.01182	1.52%	1.27E+00	9.20E-02	7.22%	7.38%
I-24	IR-73	0.25" Ni	0.01166	1.54%	5.64E-01	4.23E-02	7.49%	7.65%
B-9	IR-67	0.25" Ag	0.01453	1.24%	8.60E+01	3.19E+00	3.71%	3.91%
B-10	IR-68	0.25" Ag	0.01454	1.24%	1.31E+02	4.05E+00	3.09%	3.33%
B-12	IR-69	0.25" Ag	0.01436	1.25%	1.34E+02	4.60E+00	3.44%	3.66%
I-21	IR-70	0.25" Ag	0.01453	1.24%	3.85E+01	1.01E+00	2.63%	2.91%
I-22	IR-71	0.25" Ag	0.01476	1.22%	1.17E+02	4.50E+00	3.85%	4.04%
I-23	IR-72	0.25" Ag	0.01468	1.23%	1.20E+02	4.24E+00	3.54%	3.75%
I-24	IR-73	0.25" Ag	0.01469	1.23%	4.22E+01	1.62E+00	3.83%	4.02%

Table VI. Results of cycle CiC-7 (NT-6-3).

Location	*Holder*	*Material*	*Mass (g)*	*Mass Unc. (%)*	*Specific Activity (uCi/g)*	*2σ Std. Dev. (uCi/g)*	*2σ Std. Dev. (%)*	*Combined 2σ (%)*
B-9	IR-78	0.5" 0.1% Co	0.02386	0.75%	4.09E-01	2.31E-02	5.66%	5.85%
B-10	IR-79	0.5" 0.1% Co	0.02303	0.78%	4.32E-01	2.99E-02	6.91%	7.08%
B-12	IR-80	0.5" 0.1% Co	0.02461	0.73%	4.47E-01	2.90E-02	6.49%	6.66%
I-21	IR-91	0.5" 0.1% Co	0.0244	0.74%	2.70E-01	1.84E-02	6.80%	6.96%
I-22	IR-92	0.5" 0.1% Co	0.02418	0.74%	3.31E-01	1.51E-02	4.56%	4.80%
I-23	IR-93	0.5" 0.1% Co	0.02395	0.75%	3.36E-01	1.84E-02	5.47%	5.67%
I-24	IR-94	0.5" 0.1% Co	0.02341	0.77%	2.91E-01	1.66E-02	5.69%	5.90%
B-9	IR-78	0.25" Ni	0.01251	1.44%	4.76E+00	2.54E-01	5.34%	6.07%
B-10	IR-79	0.25" Ni	0.01298	1.39%	5.15E+00	3.17E-01	6.15%	6.74%
B-12	IR-80	0.25" Ni	0.01365	1.32%	5.21E+00	2.95E-01	5.66%	6.25%
I-21	IR-91	0.25" Ni	0.0142	1.27%	6.11E-01	3.52E-02	5.76%	6.29%
I-22	IR-92	0.25" Ni	0.01279	1.41%	7.48E-01	4.74E-02	6.34%	6.94%
I-23	IR-93	0.25" Ni	0.01404	1.28%	7.73E-01	3.99E-02	5.16%	5.76%
I-24	IR-94	0.25" Ni	0.0126	1.43%	6.62E-01	4.64E-02	7.01%	7.57%
B-9	IR-78	0.25" Ag	0.01514	1.19%	9.22E+01	3.46E+00	3.75%	4.44%
B-10	IR-79	0.25" Ag	0.0158	1.14%	9.78E+01	2.66E+00	2.72%	3.55%
B-12	IR-80	0.25" Ag	0.01496	1.20%	1.00E+02	3.16E+00	3.15%	3.96%
I-21	IR-91	0.25" Ag	0.01477	1.22%	5.52E+01	1.71E+00	3.11%	3.95%
I-22	IR-92	0.25" Ag	0.01518	1.19%	6.79E+01	2.31E+00	3.40%	4.14%
I-23	IR-93	0.25" Ag	0.0151	1.19%	6.77E+01	2.68E+00	3.95%	4.62%
I-24	IR-94	0.25" Ag	0.01455	1.24%	5.97E+01	1.99E+00	3.33%	4.15%

4 Conclusions

The objective of these measurements was two-fold. First, the qualitative comparison of the impact on neutron energy spectra in the large-B and small-I positions was desired. The hypothesis was that both positions would be impacted by the rotation of the OSCCs. Therefore, it is meaningful to discover that while indeed the small-I positions were significantly impacted by the OSCC rotation, the large-B positions were not. The impact on the small-I positions, indicated in Tabel VII below, is more understandable after observing that the rotation of the OSCCs reduces the shadowing of the hafnium absorbers on the irradiation position as they deviate from the nominal position. Therefore, as the OSCCs are rotated out, the number of thermal neutrons reaching the small-I positions increases. This is important for experiments that are deployed in these positions because the general trend at ATR is for the OSCCs to rotate out during the cycle to maintain the desired power split as fuel burns up. In contrast, no impact was observed in the large-B positions. It was hypothesized that the proximity of these positions to the OSCCs would create an impact from the backscatter of neutrons through the beryllium reflector. This observation suggests that 'penalties' assigned to experiments in these large-B positions to account for an assumed change in thermal neutron flux during the irradiation may be unnecessarily conservative. The OSCCs only ranged from 33-78 degrees during these experiments. The trailing edge of the hafnium is still present by the large B-position, but shifted away from the small-I. It is hypothesized that the thermal flux was perturbed by the hafnium at the large B-positions diminishing any shift in those positions. Additionally, the OSCC position changes the power distribution in the lobes, shifting power toward the corners for CiC-7 (on the north side). Table VII reflects the power shift with the increased fast flux and the reduced thermal/epithermal absorption in hafnium since that increases more than the fast

flux. Further investigation is necessary to determine if adjustments to these penalties is appropriate.

Table VII. Ratio of CiC-6 and CiC-7 specific activity measurements.

Location	*Relative Location*	*Material*	*Power Ratio*	*Ratio (7/6)*	*Power Normalized*	*Combined 2σ (%)*
B-9	N	0.5" 0.1% Co	0.98	1.0557	1.0828	8.83%
B-10	E	0.5" 0.1% Co	0.79	0.7406	0.9375	9.98%
B-12	W	0.5" 0.1% Co	0.84	0.7377	0.8834	8.61%
I-21	*NE*	*0.5" 0.1% Co*	*0.94*	*1.4376*	*1.5294*	*9.31%*
I-22	*SE*	*0.5" 0.1% Co*	*0.64*	*0.5766*	*0.9010*	*8.02%*
I-23	*SW*	*0.5" 0.1% Co*	*0.66*	*0.5738*	*0.8694*	*7.86%*
I-24	*NW*	*0.5" 0.1% Co*	*1.01*	*1.4096*	*1.3956*	*8.83%*
B-9	N	0.25" Ni	0.98	1.0202	1.0463	7.89%
B-10	E	0.25" Ni	0.79	0.7790	0.9860	8.48%
B-12	W	0.25" Ni	0.84	0.7769	0.9304	9.08%
I-21	NE	0.25" Ni	0.94	1.1666	1.2411	8.58%
I-22	SE	0.25" Ni	0.64	0.6085	0.9508	9.52%
I-23	SW	0.25" Ni	0.66	0.6070	0.9197	9.36%
I-24	NW	0.25" Ni	1.01	1.1730	1.1613	10.76%
B-9	N	0.25" Ag	0.98	1.0719	1.0994	5.92%
B-10	E	0.25" Ag	0.79	0.7471	0.9457	4.87%
B-12	W	0.25" Ag	0.84	0.7490	0.8970	5.39%
I-21	*NE*	*0.25" Ag*	*0.94*	*1.4346*	*1.5262*	*4.90%*
I-22	*SE*	*0.25" Ag*	*0.64*	*0.5815*	*0.9086*	*5.79%*
I-23	*SW*	*0.25" Ag*	*0.66*	*0.5660*	*0.8575*	*5.95%*
I-24	*NW*	*0.25" Ag*	*1.01*	*1.4137*	*1.3997*	*5.78%*

Furthermore, a comparison of the power-corrected ratio of thermal-to-fast neutron response (by comparing the cobalt activation to nickel) was desired to compare with simulation estimates. The ratios in Table VIII, below, demonstrate the shift in neutron spectrum in the small-I positions. The difference in these ratios for the small-I positions (bolded) support the prior observation that the neutron energy spectra in the small-I positions experience a dramatic shift towards thermalization as the OSCCs rotate out while the large-B positions are relatively unaffected by the rotation of the OSCCs. Additionally, the ratio of activity of the cobalt dosimeter to the silver dosimeter remained relatively constant in all positions. This suggests that the thermalization rate in these positions is unaffected by the OSCC rotation. The most relevant comparison however is between the calculated activity of the dosimeters from simulations and the measured activity.

Table VIII. Summary of power-corrected measurement ratios by position.

Position	*Region*	*Co/Ag*	*2σ*	*Co/Ni*	*2σ*	*Ag/Ni*	*2σ*
B-9	N	0.98	10.63%	1.03	9.86%	1.05	9.86%
B-10	E	0.99	11.11%	0.95	9.78%	0.96	9.78%
B-12	W	0.98	10.16%	0.95	10.57%	0.96	10.57%
I-21	NE	1.00	10.52%	**1.23**	9.88%	**1.23**	9.88%
I-22	SE	0.99	9.89%	0.95	11.14%	0.96	11.14%
I-23	SW	1.01	9.86%	0.95	11.09%	0.93	11.09%
I-24	NW	1.00	10.55%	**1.20**	12.21%	**1.21**	12.21%

An extensive simulation and modelling campaign is accompanying these measurements [8]. Although the full results of these simulations are not presented herein, a comparison of the computational predicted dosimeter activities to the experimentally measured activities can provide insight into the overall validity of the computations. One key step in the

computational method is the scaling of the normalized results. For the scope discussed herein, the power scaling of the computation was based on the measured cobalt results in the large-B positions. Comparisons (C/E) of the cobalt, silver, and nickel wires for both CiC-6 and CiC-7 were all made, summarized in Table IX.

Table IX. Comparison of computational and experimental dosimeter wire activities for CiC-6 and CiC-7.

Position	*Cobalt*		*Silver*		*Nickel*	
	CiC-6	*CiC-7*	*CiC-6*	*CiC-7*	*CiC-6*	*CiC-7*
B-9	0.99+/-0.09	0.94+/-0.07	0.95+/-0.05	0.93+/-0.04	0.85+/-0.08	0.82+/-0.06
B-10	1.01+/-0.09	0.99+/-0.08	1.00+/-0.05	1.00+/-0.04	0.79+/-0.07	0.81+/-0.06
B-12	0.94+/-0.07	0.96+/-0.07	0.94+/-0.05	0.96+/-0.04	0.80+/-0.08	0.82+/-0.06
I-21	1.04+/-0.08	0.98+/-0.08	1.03+/-0.05	0.98+/-0.04	0.85+/-0.08	0.82+/-0.06
I-22	1.05+/-0.09	1.06+/-0.12	1.05+/-0.05	1.08+/-0.05	0.96+/-0.22	0.78+/-0.10
I-23	1.02+/-0.07	1.05+/-0.08	1.03+/-0.05	1.09+/-0.05	0.84+/-0.15	0.82+/-0.10
I-24	1.04+/-0.09	1.05+/-0.13	1.04+/-0.06	1.05+/-0.05	0.85+/-0.15	0.82+/-0.09

While the C/E for cobalt wires in the large-B positions is trivial (because the power scaling of the computation was based on these results), there are several other noteworthy comparisons. Table IX shows that the simulation is correctly predicting Co and Ag wire activity in the large-B and small-I positions. However, the computation appears to under-predict the Ni wire activities in all cases. This suggests that the absolute normalization of the Ni wires is inaccurate or that there is a disparity in the nuclear data used. Fast neutrons are of great interest to most experimental irradiations in ATR. The computational uncertainties for Ni wire activities in the small-I positions is relatively large because the fast-neutron flux in those regions is low; efforts are ongoing to reduce these variances. In all cases there could be modelling errors, but these initial results demonstrate the importance of dosimetry measurements to compliment predictive modelling.

Even with these comparisons between simulated and measured dosimeter activities, several challenges remain when attempting to assess the impact of OSCC rotation on experiments deployed in the large-B and small-I positions in ATR. Although these measurements attempt to normalize comparison between two cycles with vastly different OSCC positions (and therefore substantially different total core powers) the fact that total core power is measured by thermal water measurements and that lobe power is correlated to un-scattered neutron fluence activation of ^{16}N in water complicates extrapolation of these measurements to other core power distributions. Similarly, these measurements compared the relative activation of thermal- and fast-sensitive dosimeters at relatively low-power and with no appreciable burn-up in the reactor. During a typical full-cycle irradiation, the burn-up of the fuel could also become a significant factor. Finally, these measurements all took place during steady-state irradiations. A more meaningful measurement would compare the response of fast and thermal sensitive sensors in real-time, however no such instruments are presently available.

This work, presented at the International Symposium on Reactor Dosimetry, May. 21-26, 2023, was supported by the United States Department of Energy Contract Number: DE-AC07-05ID14517. This information was prepared as an account of work sponsored by an agency of the U.S. Government. Neither the U.S. Government nor any agency thereof, nor any of their employees, makes any warranty, expressed or implied, or assumes any legal liability or responsibility for the accuracy, completeness, or usefulness, of any information, apparatus, product, or

process disclosed, or represents that its use would not infringe privately owned rights. References herein to any specific commercial product, process, or service by trade name, trademark, manufacturer, or otherwise, does not necessarily constitute or imply its endorsement, recommendation, or favoring by the U.S. Government or any agency thereof. The views and opinions of authors expressed herein do not necessarily state or reflect those of the U.S. Government or any agency thereof. The authors wish to express particular thanks to all of the support personnel involved in the ATR nuclear testing campaign that required participation by hundreds of skilled operators and technicians spanning numerous laboratory organizations. Special gratitude is given to the RML technicians who conducted over 2000 gamma-spectroscopy measurements to support this work: Billy Walker, Sally Louk, Larry Smith, and Christopher Jones.

References

[1] N. Manwaring, "ECAR-6479: Low-power Nuclear Testing for Reflector VII in the Advanced Test Reactor, Following the 2021 Core Internals Changeout," Idaho National Laboratory, 2023

[2] Idaho National Laboratory, "ATR Core Cross Section Diagrams, DWG-606000," 2013

[3] ASTM Standard E481, "Standard Test Method for Measuring Neutron Fluence Rates by Radioactivation of Cobalt and Silver," 2016. [Online]. Available: https://www.astm.org/e0481-16.html

[4] ASTM International Standard E264, "Standard Test Method for Measuring Fast-Neutron Reaction Rates by Radioactivation of Nickel," 2019. [Online]. Available: https://www.astm.org/e0264-19.html

[5] A. Trkov, P.J. Griffin, S.P. Simakov, L.R. Greenwood, K.I. Zolotarev, R. Capote, D.L. Aldama, V. Chechev, C. Destouches, A.C. Kahler, C. Konno, M. Kostal, M. Majerle, E. Malambu, M. Ohta, V.G. Pronyaev, V. Radulovic, S. Sato, M. Schulc, E. Simeckova, I. Vavtar, J. Wagemans, M. White, and H. Yashima, "IRDFF-II: A New Neutron Metrology Library," *Special issue of Nuclear Data Sheets,* vol. 163, pp. 1-108, 2020

[6] N. Soppera, M. Bossant, and E. Dupont, " JANIS 4: An Improved Version of the NEA Java-based Nuclear Data Information System," *Nuclear Data Sheets,* vol. 120, pp. 294-296, 2014

[7] E. Browne and J. K. Tuli, "Nuclear Data Sheets 114, 1849," 2013

[8] D. P. Griesheimer, et. al., "MC21 v.6.0 – A continuous-energy Monte Carlo particle transport code with integrated reactor feedback capabilities," Annals of Nuclear Energy, Vol. 82, 2015, pp. 29-40